SEGMENTATION OF PATIENT SPECIFIC MEG/EEG SKULL, SCALP, AND BRAIN MODELS FROM MRI

Belma Dogdas, David W. Shattuck, and Richard M. Leahy
Signal and Image Processing Institute,
University of Southern California, LA, CA 90089-2564

ABSTRACT

We present an automated method for segmenting skull, scalp, and brain regions in T1-weighted MR images of the human head that are suitable for MEG and EEG source modeling. These segmentation results can be used to generate surface and volume tessellations suitable for finite element method (FEM) or boundary element method (BEM) forward field calculations. We first segment the brain from the head using our Brain Surface Extractor software. We then use a combination of thresholding and morphology to produce a scalp mask. The brain and scalp masks provide boundaries between which the skull must lie and allow us to quickly exclude exterior voxels with intensities similar to those of the skull. We find the inner and outer skull boundaries using thresholding and morphological operations. We then mask these results with the scalp and brain volumes to ensure closed and nonintersecting skull boundaries. We have applied our segmentation algorithm to several MR images and validated our method using coregistered CT-MR image data sets.

1. INTRODUCTION

Magnetoencephalography (MEG) and electroencephalography (EEG) inverse problems require realistic models of the head for use in accurate computation of the mapping from neural current sources to scalp potentials and extracranial magnetic fields [2]. Because of the existence of closed form solutions for the MEG and EEG forward problem, multilayer spherical models have traditionally been used to approximate the human head with a set of nested spheres representing brain, skull and scalp. Recently, representations of the head as a set of contiguous regions bounded by surface tessellations of the scalp, outer skull, inner skull, and brain boundaries have been used as a more realistic model. Using boundary element methods in conjunction with these models produces more accurate results than the multilayer spherical model but requires that a volumetric image of the subject's head first be segmented into its component bone and soft tissue regions.

The CT-MR image data sets were provided as part of the project, "Retrospective Image Registration Evaluation", National Institutes of Health, Project Number 1 R01 CA89323, Principal Investigator, J. Michael Fitzpatrick, Vanderbilt University, Nashville, TN. We thank Dr. Colin Studholme for providing 3D Multi-model Image Registration Viewer (RView) software 8.0w Beta [1]. This work was supported by NIMH Grant RO1-MH53213 and NCRR Grant P41-RR13642.

2. OBTAINING ANATOMICAL SURFACES OF BRAIN, SCALP AND SKULL

We segment the brain using the Brain Surface Extractor (BSE) software, v.3.0. BSE identifies the brain using anisotropic diffusion filtering, Marr-Hildreth edge detection, and morphological operations. Anisotropic diffusion filtering improves edge definition in the MR image by smoothing non-essential gradients in the volume without blurring steep edges. The Marr-Hildreth edge detector identifies important anatomical boundaries such as the brain-skull boundary. The brain is identified and refined using a sequence of morphological and connected component operations [3].

To segment the scalp, we first apply simple thresholding to identify the boundary between the skin and surrounding air [4]. We compute an empirical skull threshold as the mean of the histogram after extraction of the brain, and we estimate the scalp threshold as the mean of the histogram above the skull threshold. These thresholds give the algorithm an initial estimate of the range of the skull and scalp intensities. They may be adjusted by the user to improve the segmentation. After thresholding, the volume will still contain background voxels due to noise and regions inside the head which have low intensity values. To address these problems, we apply a modified morphological closing operation which performs a hole filling between dilation and erosion. This hole-filling closing operation will have the effect of filling any cavities that are disjoint from the background after dilation, forming a single volume that contains the entire head. We select the largest foreground connected component as the head volume and remove the remaining noise by applying an opening operation with a cube of size 2 voxels (C_2) to the resultant volume.

To find the outer skull we begin by labeling the dark voxels in the image with a thresholding operation. We estimate a threshold for skull as the mean of the histogram of the non-zero voxels in the MR volume that are not identified as brain. After thresholding, the regions which were not included in the skull volume are filled by taking the union of our thresholded image with a dilated brain mask. Next, we take the intersection of this volume with a modified scalp volume to include only the dark voxels that lie within the head. We obtain this modified scalp volume by applying an opening operation with a cube structuring el-

ement of size 12, followed by an erosion operation with a cube of size 1 as the structuring element. These two operations generate a modified scalp volume that typically does not include the ears and nose. The largest connected region resulting from the intersection operation will be the closed volume bounded by the outer skull, but may contain additional connected components such as the eyeballs. Thus we now select the largest connected component. We then close the boundary of the outer skull using a closing operation with a 3D octagonal structuring element of size 4 voxels (O_4) [4]. This closing operation may cause the volume to intersect the scalp, so our final operation is to again mask the volume with the eroded scalp to enforce the physical constraint that the outer skull boundary lies within the scalp. The resulting volume is a closed volume bounded by the outer skull boundary.

To find the inner skull, we first mask the MR image with a skull mask that we obtain from the outer skull volume by erosion with a cubic structuring element of size one voxel to ensure that the inner skull will lie inside the outer skull. Then, using the same threshold as for the outer skull, we remove the skull from this volume by applying a thresholding operation. Then we take the union of this volume with a dilated brain mask to fill holes in the volume that are due to CSF voxels with intensities similar to those of the skull. Next we perform the opening operation to remove diploic fat and other extraneous materials using structuring element O_4. While the previous steps will remove most CSF from the estimated skull mask, there may be regions where the dilated brain mask alone does not encompass all CSF, which therefore appears as part of the skull. To overcome this problem we impose a physical constraint on skull thickness in our algorithm and make sure that the skull volume does not exceed 4mm. We apply an erosion operation to the outer skull volume using a structuring element of O_4 and obtain the inner skull after masking the volume with this eroded skull. While this operation will lead to underestimation of skull thickness in subjects with thicker skulls, it is a practical solution to the problem that CSF and skull are often indistinguishable. This thickness constraint can also be modified by the user.

Finally, we modify our segmentation results to ensure that the brain, skull and scalp are strictly nested within each other. First we dilate the brain mask with structuring element C_1 and take the union of this mask with the inner skull. We repeat the same procedure for the outer skull and scalp. We obtain the outer skull by taking its union with the dilated inner skull; we obtain the scalp by taking its union with the outer skull dilated with structuring element C_1.

3. RESULTS

We implemented our segmentation algorithm using C++. We applied our scalp, skull, and brain segmentation algorithm to more than 40 MR images and validated it using 8 coregistered CT-MR data sets [5]. The dimensions of the MR data were 256 x 256 x 128 with resolution on the average of 0.98mm x 0.99mm x 1.484mm. The corresponding CT scans had 3mm slice thickness with slice dimensions 512 x 512, with resolution on the average of 0.419mm x 0.419mm. The number of slices for each volume varied between 42 and 49. We processed the CT and MR volumes by registering each CT volume to its corresponding MR image. We registered these data using the 3D Multi-Modal Image Registration Viewer Software (RView 8.0w Beta) [1]. After aligning the volumes, we labeled the skull in the CT data sets using a thresholding operation. We used closing and flood filling procedures to fill the diploic spaces within the skull. We also labeled the scalp and brain in CT data sets using morphological operations. We treat the segmentation results which we get from CT as a gold standard against which to compare the MR segmentations. Fig 1 shows results of the segmentation of brain, skull and scalp from MRI and its corresponding CT data for transaxial, sagittal and coronal sections. Fig 2 shows the results as tessellations of the scalp, outer skull, inner skull and brain for one of the MR data sets.

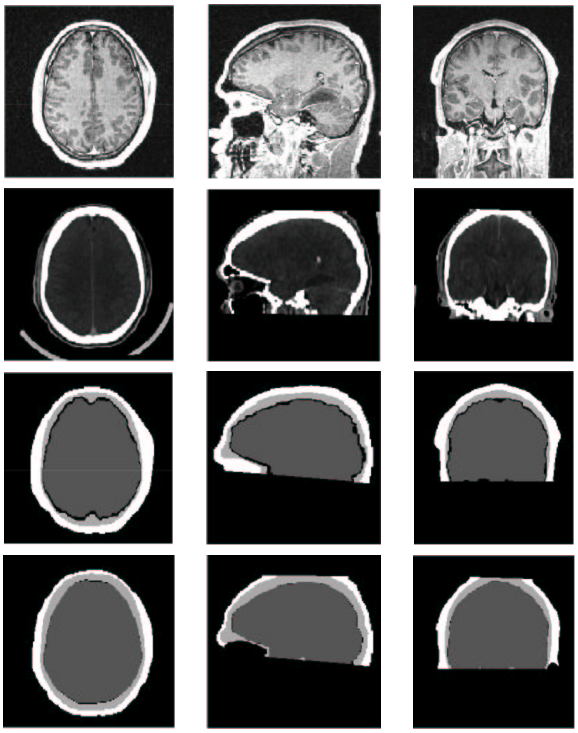

Fig. 1. Segmentation of brain, skull and scalp from MRI and its corresponding CT on transaxial, sagittal and coronal slices respectively. First Row: Original MR image. Second Row: Original CT data. Third Row: Segmentation of brain, skull and scalp from MRI. Fourth Row: Segmentation of brain, skull and scalp from CT.

To assess the performance of our algorithm we computed the Dice coefficients between regions obtained from the CT and MR images [4].

Skull morphology in the lower portion of the head is extremely complex and performance of our algorithm in these regions is unreliable. However, forward modeling calculations in MEG and EEG are primarily affected by

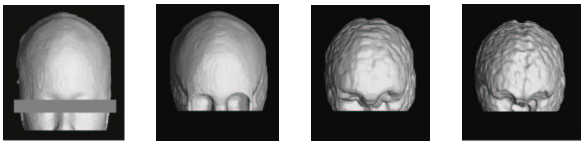

scalp outer skull inner skull brain

Fig. 2. Surface tesselations of the scalp, outer skull, inner skull, and brain obtained from one of the MR data sets

	Brain	Skull	Scalp
Patient1	0.9241	0.7608	0.682
Patient2	0.9309	0.7134	0.7665
Patient3	0.9674	0.6364	0.6123
Patient4	0.8406	0.7940	0.7228
Patient5	0.9209	0.7852	0.7752
Patient6	0.9516	0.7912	0.7488
Patient7	0.9008	0.7254	0.7924
Patient8	0.9058	0.7964	0.6832
Average	0.9178 ± 0.038	0.7504 ± 0.056	0.7229 ± 0.061

Table 1. Dice coefficients comparing brain, skull volumes (i.e., the region between inner and outer skull boundaries) and the region between outer skull and scalp boundaries for eight coregistered CT and MR image data sets.

the scalp and the skull boundaries in the regions above the plane passing through the nasion and inion and perpendicular to the sagittal planes. Consequently, we restricted our evaluation to the volumes above this plane. We compared each brain, skull (the region between the outer and the inner skull boundaries) and the region between the outer skull and the scalp boundaries obtained from the MR image with the corresponding structure extracted from the coregistered CT. Table 1 lists the Dice coefficients for the 8 MR/CT data sets used in this study.

To assess the implications of the results in Table 1, we compared these values with the Dice coefficients and set differences computed from misregistered copies of the CT skull for one of the CT/MR data sets. Set differences are computed as:

$$diff(S_1, S_2) = \frac{|S_1| - |S_1 \cap S_2|}{|S_1|} \quad (1)$$

In this way we can compute the degree of misregistration between a CT image and the head which would account for a similar level of error as that between our CT gold standard and the MR skull. We shifted the CT skull volume by 1mm separately along each of the three cardinal axes in turn. We also shifted the skull volume by 1mm, 2mm and 3mm along each of the three axes to create an additional three misregistered skull volumes. These latter three volumes correspond to shifts by $\sqrt{3}$, $2\sqrt{3}$ and $3\sqrt{3}$mm. We then computed the Dice coefficients and set differences between these shifted and original CT skulls. Table 2 lists the Dice coefficients and set differences for these comparisons for one of the data sets. These results reveal that CT/MR errors are comparable to misregisration on the order of 1.7mm between an accurately determined CT-based skull and the subject's head. We can therefore conclude that our algorithm generates scalp and skull volumes that may be of acceptable accuracy for MEG and EEG source modeling since registration errors on the order of 1-2mm are typical for these modalities.

$S_1 \; vs \; S_2$	$Dice \; Coefficient$	$diff(S_1)$	$diff(S_2)$
$MRI \; vs \; CT$	0.7964	0.1991	0.1818
$CT \; vs \; CT_{1x}$	0.9032	0.0965	0.0971
$CT \; vs \; CT_{1y}$	0.9010	0.0962	0.1018
$CT \; vs \; CT_{1z}$	0.8714	0.1286	0.1286
$CT \; vs \; CT_{1w}$	0.7925	0.2048	0.2102
$CT \; vs \; CT_{2w}$	0.6189	0.3769	0.3852
$CT \; vs \; CT_{3w}$	0.4600	0.5354	0.5445

Table 2. Table of the Dice coefficients and set differences for the comparison of 1mm, 2mm and 3mm misregistered CT skull with itself and MR skull in the direction of coronal, transaxial and sagittal sections. x corresponds to coronal, y corresponds to transaxial, z corresponds to sagittal direction and w corresponds misregisration in all directions.

In some instances one may need to adjust the scalp and skull thresholds and the parameters in Brain Surface Extractor (BSE) software to obtain improved estimates of surfaces. However, the thresholds can be quickly adjusted and identification of the scalp, skull and brain surfaces on a 256-256-128 volume using the method described here requires less than 40 seconds of processing time on a 1GHz Pentium III processor.

4. REFERENCES

[1] C.Studholme, D.L.G.Hill, and D.J.Hawkes, "An overlap invariant entropy measure of 3D medical image alignment," *Pattern Recognition*, vol. 32 1, pp. 71–86, Jan 1999.

[2] J. C. Mosher, R.M. Leahy, and P.S. Lewis, "EEG and MEG: forward solutions for inverse methods," *IEEE Transactions on Biomedical Engineering*, vol. 46 (3), pp. 245–259, March 1999.

[3] D.W. Shattuck and R. M. Leahy, "Brainsuite: An automated cortical surface identification tool," *Medical Image Analysis*, vol. 6 (2), pp. 129–142, 2002.

[4] B. Dogdas, D. W. Shattuck, and R. M. Leahy et al., "Segmentation of skull in 3D human MR images using mathematical morphology," *SPIE Proceedings*, vol. in press, 2002.

[5] J.West, J. M. Fitzpatrick, M. Y. Wang, B. M. Dawant, et al., "Comparison and evaluation of retrospective intermodality image registration techniques," *Journal of Computer Assisted Tomography*, vol. 21, pp. 554–566, 1997.